Chalcogenide Letters Vol. 17, No. 8, August 2020, p. 411 - 416

RAMAN CHARACTERIZATION OF $CuIrSnX_4$ NORMAL-SPINEL SYSTEMS

P. BARAHONA[a], A. GALDÁMEZ[b], P. VALENCIA-GALVEZ[b], S. MORIS[c,*]
[a]*Basic Science Faculty, Catholic University of Maule, San Miguel 3605, Talca 3480112, Chile*
[b]*Department of Chemistry, Science Faculty, University of Chile, Las Palmeras 3425, Santiago, 7800003, Chile*
[c]*Center of advanced investigation studies of Maule (CIEAM), Vice-rectory of research and postgraduate, Catholic University of Maule, San Miguel 3605, Talca 3480112, Chile*

$CuIrSnS_4$, $CuIrSnSe_4$ and $CuIrSnS_2Se_2$ were synthetized by a solid-state reaction at 700 °C. Powder X-ray diffraction patterns were consistent with normal spinel-type structure. Scanning electron microscopy (SEM-EDS) images showed a uniform distribution of Cu-Ir-Sn-S and Se atoms in the samples. Raman scattering analysis revealed A_{1g}, E_g, and three F_{2g} vibrational modes in spectra (cubic $Fd\bar{3}m$ space-group). Signal at ~320 cm^{-1} corresponded to the A_{1g} mode, while the band at ~ 230 cm^{-1} was assigned to the $F_{2g}(2)$ mode due to the asymmetric stretching of the Cu-X bond. Raman spectra were compared with those of the previously published thio- and selenospinels.

(Received April 15, 2020; Accepted August 10, 2020)

Keywords: Spinels, Inorganic materials, Thio- and selenospinels, Raman spectra

1. Introduction

Compounds with CuM_2X_4 (X=S, Se) spinel structure have attracted great attention due to their numerous interesting structural, magnetic, and electrical properties [1–6]. Spinels such as $CuIr_2S_4$ exhibit a temperature-induced metal-insulator (*M-I)* transition at approximately T_{M-I} =230 K with structural transformation, showing hysteresis upon heating and cooling [1],[5],[7],[8]. On the other hand, $CuIr_2Se_4$ remains metallic down to 0.5 K [9], without an *M-I* transition such as in $CuIr_2S_4$. The M-I transition induced by pressure and the instability of the metallic state in $CuIr_2Se_4$ at high pressures have been investigated [10],[11].

Raman spectroscopy is a useful technical to characterize spinel compounds. Several works on thio- and selenospinels have been published in the previous year [2],[3],[12],[13], in which the technique is used to give information about the dependence of the lattice vibrations on the tetrahedral and octahedral cations caused by slight structural distortions.

In this article, we report the Raman characterization of the $CuIrSnS_4$, $CuIrSnSe_4$ and $CuIrSnS_2Se_2$ phases; these results are compared with those of the published thio- and selenospinels to clarify how cationic and anionic substitutions affect the Raman modes.

2. Experimental section

2.1. Synthesis

Polycrystalline $CuIrSnX_4$ (X=S, Se) compounds were prepared by directly combining high-purity elemental powders (99.99%, Aldrich, USA) in stoichiometric amounts. All manipulations were carried out under an argon atmosphere. The reaction mixtures were sealed in evacuated quartz ampoules and placed in a programmable furnace. The ampoules were then slowly heated from room temperature to 700 °C and held at the maximum temperature for 7 days. Finally, the ampoules were slowly cooled from 700 °C to room temperature at a rate of 60 °C/min.

* Corresponding autor: smoris@ucm.cl

2.2. Powder X-ray diffraction measurements

Powder X-ray diffraction (PXRD) patterns were collected at room temperature on a Bruker D8 Advance diffractometer equipped with a Cu Kα radiation source in a range of $5° < 2\theta < 80°$.

2.3. SEM-EDS analysis

The chemical compositions were determined by energy-dispersive X-ray analysis using a Vega 3 Tescan system equipped with a Quantax 400 (EDS) microanalyzer. The samples were mounted onto double-sided carbon tape, which was adhered to an aluminum specimen holder.

2.4. Raman scattering measurements

Raman scattering measurements were conducted on a Witec Alpha 300 System using a 532 nm wavelength excitation. The spectrometer was calibrated with a reference single-crystal Si sample (Raman peak at 520.7 cm^{-1}). The spectral data were collected at room temperature in the backscattering configuration in a spectral range of 100-400 cm^{-1}, with a laser spot of ~1 μm and a laser power of 2 mW.

3. Results and discussion

3.1. X-ray powder diffraction and compositional characterization

The XRD patterns of the polycrystalline $CuIrSnS_4$, $CuIrSnSe_4$ and $CuIrSnS_2Se_2$ phases are shown in Fig. 1. The major XRD diffraction peaks appear at 2θ = 15.05, 29.16, 35.19, 46.40, 50.72, 53.28, 63.37, 71.24 and 74.60 and can be attributed to the (111), (311), (004), (333), (044), (315), (444), (535) and (008) hkl planes, which are in good agreement with the results for reported normal spinels [4,6]. No secondary phases or impurity peaks are detected in the XRD patterns.

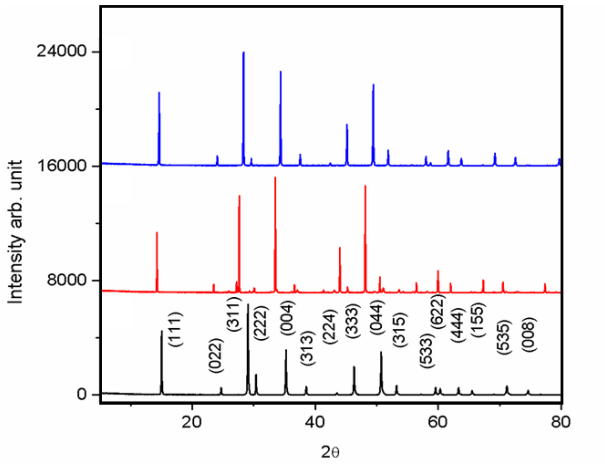

Fig. 1. X-ray powder diffraction patterns for $CuIrSnS_4$ (bottom), $CuIrSnSe_4$ (middle) and $CuIrSnS_2Se_2$ (top).

The volumes of the cell lattice for these compounds obeyed Vegard's law (Fig. 2). The volume increases gradually with the selenium content due to the substitution of S^{2-} (1.84 Å) by Se^{2-} (1.98 Å)[14]. The average grain size, which is determined from grazing incidence XRD using the Debye–Scherrer formula [15] with the full width at half maximum of the (111) diffraction peak, is ~80 nm.

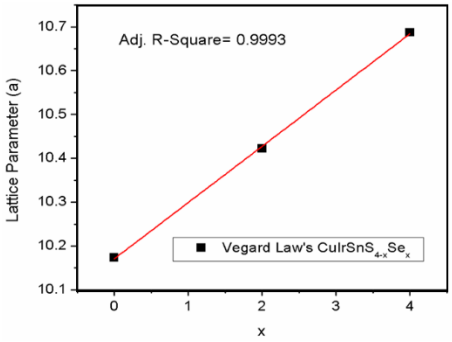

Fig. 2. Vegard's Law for $CuIrSnS_{4-x}Se_x$.

The chemical compositions of the powder samples were determined using EDS analysis on the polished surfaces of sample pellets. The backscattered image and EDS analysis (chemical maps of several areas) reveal that the samples are uniform throughout the scanned regions. Fig. 3 shows a representative SEM-EDS analysis. The experimental results reveal that the ratio Cu/Ir/Sn/S/Se is 1.09/1.03/1.01/1.99/1.8 for the nominal $CuIrSnS_2Se_2$ composition. Based on the EDS data, the elemental mapping images are shown in Fig. 3, and Cu, Ir, Sn, S and Se are distributed uniformly in the selected area.

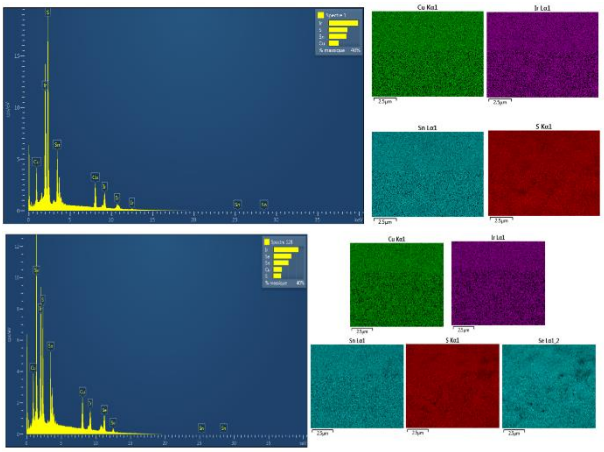

Fig. 3. Scanning electron microscopy (SEM) micrograph: EDS mapping spectral analysis of $CuIrSnS_4$ (top) and $CuIrSnS_2Se_2$ (bottom).

3.2. Raman analysis

Using this technique, measurements were made at room temperature with a 532 nm laser[16],[17]; the response for the compounds $CuIrSnS_4$, $CuIrSnSe_4$ and $CuIrS_2Se_2$ was measured in the spectral region between 100 and 400 cm^{-1}, an area where the most important changes were observed. Figure 4 shows the spectra obtained for each of the phases, and in them, four bands are clearly observed; however, by fitting the spectra with Lorentzian functions, we can perform a more detailed analysis and identify five signals, which are located at the approximate frequencies of 130, 165, 230, 265 and 320 cm^{-1}. Table 1 summarizes the vibrations observed for the compounds reported in this work and others previously reported by our group for similar solid spinel-type solutions [3], [13].

The normal spinel-type compounds crystallize in the $Fd\bar{3}m$ space group, corresponding to a face-centered cubic structure (fcc) that has an arrangement with a large unit cell, which contains eight units of the formula (8 cations A, 16 cations M and 32 anions X) [6,18]. The

structure has 17 vibrational modes, of which five of them are active in Raman, $\Gamma_R = A_{1g} + E_g + 3\ F_{2g}$ [3],[13],[16–19].

As mentioned, the synthesized compounds manifest the five characteristic modes of the $Fd\bar{3}m$ group. The vibrational mode A_{1g} is observed at ~ 320 cm^{-1} and is assigned to the symmetrical stretching of the chalcogen bond with respect to copper in the tetrahedral position [13], [19–21], while the band at ~ 230 cm^{-1} is assigned to the F_{2g} (2) mode due to the asymmetric stretching of the Cu-X bond. On the other hand, the symmetric and asymmetric flexion of the chalcogen with respect to copper is assigned to the F_{2g} (1) mode at a frequency of ~ 130 cm^{-1}.

Regarding to the modes E_g (~165 cm^{-1}) and F_{2g} (3) (~ 265 cm^{-1}), they are assigned to the symmetric and asymmetric torsions of the chalcogen on the Ir/Sn - X link at the M sites of AM_2X_4 [3], [19,20]. Brüesch and D'Ambrogio [19] have reported that, although the strength constants of the selenium and sulfur spinels differ slightly, the strength constants for the M-X bonds are very similar, regardless of the metal that occupies the tetrahedral position (A).

However, we observe a signal at ~ 320 cm^{-1} corresponding to mode A_{1g}, and signals at ~ 230 cm^{-1} and ~ 265 cm^{-1} corresponding to the vibrational modes F_{2g} (2) and F_{2g} (3), respectively, representing a lower wavelength shift with respect to those of the $CuCrSnS_2Se_2$ phase [13], which contains Cr/Sn atoms at the M position (see Table 1). The displacement of the signal is attributed to the incorporation of atoms of Ir at position M, taking into account that the atomic weight of Ir is considerably greater than the weight of Cr and that a replacement in the structure by a heavier atom leads to a shift towards a lower energy. Therefore, our results plus the point raised by Brüesch *et al*. allow us to interpret that these three modes (A_{1g}, F_{2g} (2) and (3)) show the qualitative content of iridium. The chemical interactions of Ir-chalcogen evidently influence the environment, causing changes in the polarities of the bonds that are manifested in the intensity and position of the signals for the $CuIrSnX_4$ phases (X= S, Se).

Table 1. Frequency and proposed mode assignment of Raman peaks from solid solutions of $CuCrSnS_4$, $CuCrSnS_2Se_2$ and $CuIrSnX_4$ (X= S, Se).

mode	$CuCrSnS_4$ [3]	$CuCrSnS_2Se_2$ [13]	$CuIrSnS_4$	$CuIrSnSe_4$	$CuIrSnS_2Se_2$
F_{2g} (1)	130	124	122	131	130
E_g	165	---	162	165	167
F_{2g} (2)	299	295	---	228	242
F_{2g} (3)	337	336	245	262	282
A_{1g}	379	---	320	306	347

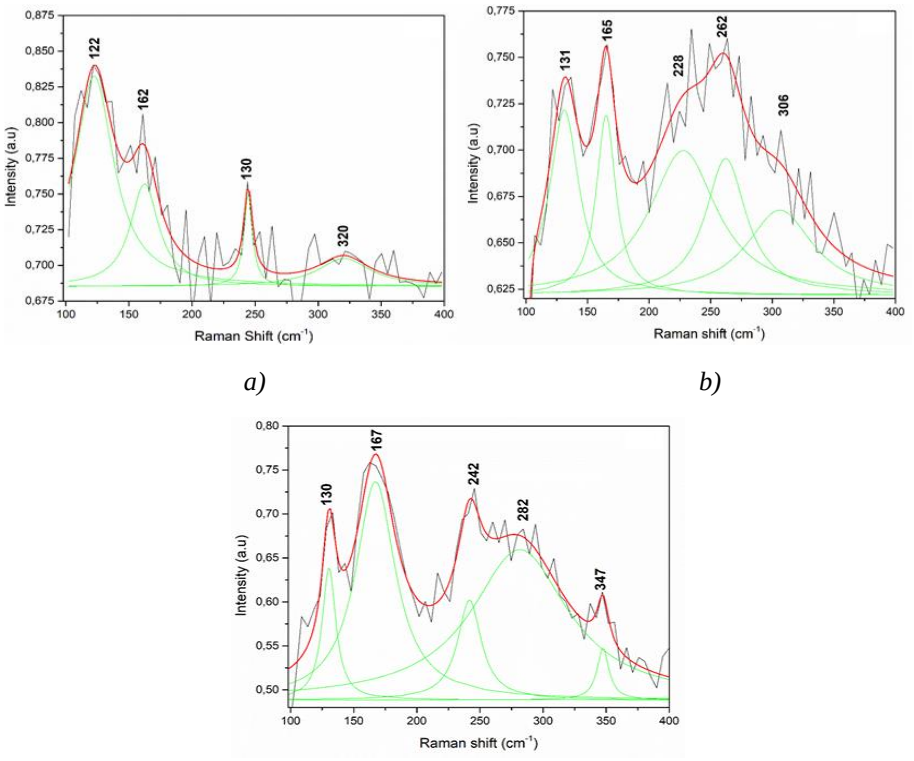

Fig. 4. Raman spectra of a) $CuIrSnS_4$, b)$CuIrSnSe_4$; c) $CuIrSnS_2Se_2$ powder samples with the different contributions, as deduced from the fitting of the different peaks with Lorentzian curves (green lines).

4. Conclusions

Samples of $CuIrSnS_4$, $CuIrSnSe_4$ and $CuIrSnS_2Se_2$ were synthesized by the conventional solid-state method. The homogeneity and stoichiometry were confirmed by SEM-EDS and powder XRD, which indicated that the samples were single phases and had homogenous distributions of elements. The vibrational analysis showed that the A_{1g}, E_g, and three F_{2g} modes were Raman-active, in good agreement with the spectra of the AM_2X_4 spinel members. Our results confirm that the Raman spectroscopy technique is very useful for identifying and characterizing these spinel systems. Raman spectra of these systems can be explained by cation/anion disorder.

Acknowledgments

The authors thank the FONDEQUIP Grant EQM140142 for the Raman Witec Alpha 300 equipment.

References

[1] N. Koseki, S. Ebisu, S. Nagata, J. Alloys Compd. **509**, 568 (2011).
[2] P. Barahona, A. Galdámez, F. López-Vergara, V. Manríquez, O. Peña, J. Solid State Chem. **212**, 114 (2014).
[3] P. Valencia-gálvez, O. Peña, S. Moris, P. Barahona, J. Chil. Chem. Soc. **64**, 4285 (2019).
[4] S. Moris, P. Barahona, A. Galdámez, Zeitschrift Für Krist. Cryst. Struct. **234**, 421 (2019).
[5] M. Ito, K. Sonoda, S. Nagata, Solid State Commun. **265**, 23 (2017).

[6] K. E. Sickafus, J. M. Wills, N. W. Grimes, J. AM. Ceram. Soc. **82**, 3279 (1999)
[7] J. Tang, T. Matsumot, T. Furubayashi, T. Kosaka, S. Nagata, Y. K, J. Magn. Magn. Mater. **181**, 1363 (1998).
[8] S. Nagata, N. Matsumoto, Y. Kato, T. Furubayashi, T. Matsumoto, J. Sanchez, P. Vulliet, Phys. Rev. B. **58**, 6844 (1998).
[9] N. Takatsugu, Hagino Yoshitaka, Seki Shoichi, Phys. C. **240**, 1303 (1994).
[10] S. Tsuji, K. Kumagai, N. Matsumoto, S. Nagata, Phys. C Supercond. **282–287**, 1107 (1997).
[11] S. Nagata, N. Matsumoto, R. Endoh, N. Wada, Phys. B Condens. Matter. **329–333**, 4 (2003).
[12] F. J. Manjon, I. Tiginyanu, V. Ursaki, Pressure-Induced Phase Transitions in AB_2X_4 Chalcogenide Compounds., Springer-V, Berlin, 2014.
[13] S. Moris, P. Valencia-Gálvez, J. Mejía-López, O. Peña, P. Barahona, A. Galdámez, Inorg. Chem. **58**, 13945 (2019).
[14] R. D. Shannon, Acta Crystallogr. Sect. A. **32**, 751 (1976).
[15] D. M. Smilgies, J. Appl. Crystallogr. **42**, 1030 (2009).
[16] S. Moris, V. Manríquez, P. Barahona, A. Galdámez, P. Valencia-Gálvez. Chalcogenide Lett. **15**, 12 (2018).
[17] S. Moris, P. Barahona, P. Valencia-Gálvez, A. Galdámez. Chalcogenide Lett. **16**, 6 (2019).
[18] C. Biagioni, M. Pasero, Am. Mineral. **99**, 1254 (2014).
[19] F. Brüesch, P., D'Ambrogio, Phys. Status Solidi B **50**, 513 (1972).
[20] V. Gnezdilov, P. Lemmens, Y. G. Pashkevich, C. Payen, K. Y. Choi, J. Hemberger, A. Loidl, V. Tsurkan, Phys. Rev. B. **84**, 1 (2011).
[21] P. Brüesch, C. Schüler, B. Boveri, J. Phys. Chem. Solids. **32**, 1025 (1971).